Near Real-Time Confocal Microscopy of Amelanotic Tissue:

Detection of Dysplasia in ex Vivo Cervical Tissue[1]

Tom Collier, MS, Alicia Lacy, BS, Rebecca Richards-Kortum, PhD, Anais Malpica, MD, Michele Follen, MD, PhD

Rationale and Objectives. The authors performed this study to determine whether images of ex vivo tissue obtained with a near real-time confocal microscope can be used to differentiate between normal and dysplastic tissue.

Materials and Methods. Biopsy specimens of colposcopically normal and abnormal cervical tissue were obtained from 19 patients and imaged at various depths with a confocal microscope. Nuclear morphologic features were extracted from the confocal images; in addition, a group of reviewers examined the images and attempted to identify whether the specimen contained high-grade dysplasia. Results of both analyses were compared with the histopathologic findings of the same specimens provided by a board-certified pathologist with expertise in gynecologic pathology.

Results. The morphologic feature measurements compared well with the findings at pathologic examination. The use of the nuclear-cytoplasmic ratio to determine the presence of dysplasia resulted in a sensitivity of 100% and a specificity of 91%. The untrained reviewers had an average sensitivity of 95% and an average specificity of 69% in the determination of dysplasia.

Conclusion. The results indicate the clinical potential of in vivo confocal imaging in the detection of dysplasia.

Key Words. Uterus, abnormalities; uterus, biopsy.

© AUR, 2002

Invasive carcinomas of the uterine cervix, urinary bladder, respiratory tract, oral mucosa, skin, and colon are preceded by precancerous changes within the epithelium. Despite the presence of precursor lesions, the mortality rate for patients with these cancers is substantial (1). Early detection represents the best opportunity to improve patient survival and quality of life; thus, new surveillance methods are needed to improve the ability to recognize precancerous changes within epithelial tissues. The precancerous epithelium is associated with a variety of morphologic alterations, including increased nuclear size, increased nuclear-cytoplasmic ratio, nuclear hyperchromasia, and pleomorphism (2).

Confocal imaging has been proposed as a new tool to noninvasively assess cell morphology by using light reflected from tissue (3–10). A pinhole placed at a conjugate image plane in the confocal microscope is used to localize reflected light in three dimensions with sufficient resolution to image individual cells and nuclei. Changes in the refractive index provide the contrast necessary to recognize intracellular detail. In concept, this is similar to the histologic analysis of biopsy specimens, except that three-dimensional resolution is achieved without removing or physically sectioning tissue. Thus, confocal imaging provides a potential tool for detecting precancerous changes in the intact epithelium. Confocal images can

Acad Radiol 2002; 9:504–512

[1] From the Department of Electrical and Computer Engineering, the University of Texas at Austin, ENS 610, Austin, TX 78712 (T.C., A.L., R.R.K.), and the Departments of Pathology and Gynecologic Oncology, the University of Texas M.D. Anderson Cancer Center, Houston, Tex (A.M., M.F.). Received November 6, 2001; accepted January 9, 2002. Supported by National Institutes of Health grant RO1 CA 82880-01. **Address correspondence to** T.C.

© AUR, 2002

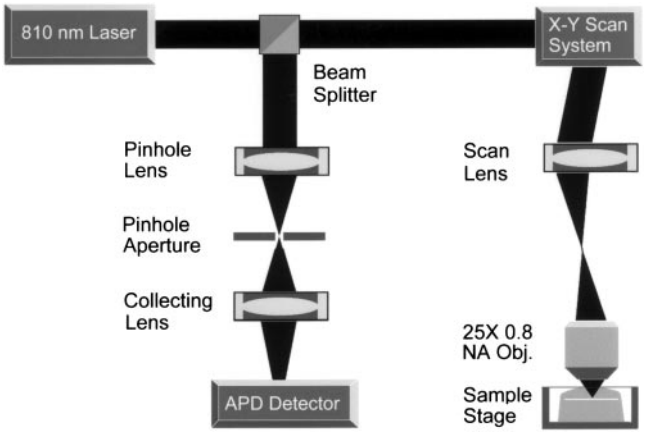

Figure 1. Diagram of confocal microscope system. The 810-nm diode laser sends a beam through a beam splitter to the x-y scan system, which raster scans the beam across the scan lens. This lens focuses the beam onto the back focal length of the objective (*NA Obj.*). The light is reflected off the tissue back through the scan system, which descans the beam. This signal light is then reflected off the beam splitter, through the pinhole aperture, and detected by the avalanche photodiode (*APD*).

also be obtained in near real time, thus enhancing its potential use in a clinical setting for directing biopsy.

To date, much of the work with in vivo confocal imaging has focused on the eye (3–5) and skin (6–10), organ sites that are easily accessible with fixed conventional microscopes. Our group is developing a fiberoptic confocal endoscope for in vivo imaging of less accessible organs such as the uterine cervix (11). The system has been designed to image subcellular detail of these amelanotic tissues for the in situ detection of abnormalities. A fiberoptic imaging bundle is incorporated into the system to provide the necessary flexibility to image organ sites not accessible with conventional confocal systems.

The most promising use for real-time confocal systems has been in the imaging of human skin, where melanin, with its high refractive index of 1.7, provides the primary source of contrast for imaging individual cells (8). We have previously shown (12–14) that confocal images of amelanotic cells have inherently less contrast than do those of cells with melanin. When epithelial cells (13) and previously frozen tissue (14,15) are treated with weak acetic acid, however, the backscattering associated with the nucleus increases, which provides additional contrast on confocal images sufficient for quantitative nuclear morphometry (15). Acetic acid is commonly used to aid in the detection of precancerous changes in the cervix (16).

To assess the potential of the fiberoptic confocal microscope in the in vivo detection of abnormalities, we performed this study to determine whether confocal images of fresh cervical biopsy specimens obtained with a near real-time nonfiber prototype system could be used to identify the presence of precancerous changes in the cervix.

MATERIALS AND METHODS

Patients

Cervical biopsy specimens were obtained from 25 patients at the colposcopy clinics of the University of Texas M.D. Anderson Cancer Center, Herman Hospital, and Lyndon Baines Johnson Hospital in Houston, Tex. The patients had been referred to these clinics (*a*) because they were suspected of having dysplasia owing to abnormal findings at cervical cytologic examination or (*b*) for removal of the cervical tissue with the loop electrical excision procedure owing to a previous diagnosis of dysplasia. Informed consent was obtained from the patients, and the project was reviewed and approved by the Surveillance Committee at the University of Texas M.D. Anderson Cancer Center and the Institutional Review Board at the University of Texas at Austin. Five patients were excluded from the study owing to unsuccessful acquisition or histologic processing of one of the two biopsy specimens. An additional patient, with only focal dysplasia at histologic examination of one of the biopsy specimens, was excluded because it was believed that the probability of a meaningful correlation between the histologic diagnosis and the confocal images was remote.

Confocal System

We designed and built an epi-illumination confocal microscope (12) (Fig 1). The light source is a continuous-wave diode laser operating at 810 nm. The scanning mirrors are driven by a pair of galvanometers to produce a frame rate of 7.5 Hz (4,000-kHz Video Scan Head; General Scanning, Boston, Mass). The scanning lens focuses the beam at the back focal plane of a ×25 0.8 NA (numerical aperture) water immersion objective (Plan-Neofluar multi-immersion; Zeiss, Thornwood, NJ); 10–30 mW of power is focused to a 1-μm-diameter spot on the sample. Light backscattered from the tissue returns to the beam splitter, where it is reflected to the pinhole lens and focused through a 10-μm-diameter pinhole aperture. Light that passes through this pinhole is detected by an avalanche photodiode. The confocal system operates at a di-

mensionless pinhole radius of 2.5 to provide maximum optical sectioning for obtaining cellular detail. The scanning system is capable of scanning at variable angle ranges, thus providing zoom capability. The measured lateral and axial resolution of the system are 0.8 and 2–3 μm, respectively.

Specimens

Two uterine cervix biopsy specimens were obtained from each patient. One of the specimens was obtained from a normal area of the cervix and the other was taken from an abnormal area, as determined by the clinician using colposcopy, and immediately placed in growth medium (Dulbecco's Modified Eagle Medium, no phenol). The colposcopic appearance (ie, normal or abnormal) was recorded for each biopsy specimen. The biopsy specimens were approximately 3 mm wide, 4 mm long, and 2 mm thick. The specimens underwent confocal imaging within 6 hours of excision.

Imaging

The specimens were removed from the growth medium and rinsed with phosphate buffered saline. A 6% solution of acetic acid was then added to each sample, and images were acquired at various epithelial depths up to the working distance of the microscope (250 μm). Confocal images were obtained with the image plane parallel to the tissue surface. Images were digitized by using a video frame grabber card and displayed at 7.5 frames per second on a computer monitor. Individual bitmap image files were saved from the frame grabber's video buffer. All samples were submitted for routine histologic examination after staining with hematoxylin-eosin. Sections were examined by an experienced, board-certified gynecologic pathologist (A.M.).

Image Processing

Each of the single frames presented herein was resampled and processed to enhance the brightness and contrast. The brightness and contrast were increased by 17% and 53%, respectively. Brightness was enhanced by adding the noted percentage of full gray scale to each pixel; contrast was enhanced by removing the noted percentage of full gray scale from the image and expanding the remaining midrange gray levels. Resampling was performed to reduce the distortion on the images caused by nonlinearity in the resonant galvanometric scanning system. Linear interpolation was used to estimate pixel values. Morphologic nuclear features, including nuclear area, nuclear diameter, nuclear density, and nuclear-cytoplasmic ratio were extracted from each image. Nuclear masks were created by visual recognition of one operator (T.C.), who was blinded to the histologic and colposcopic results, by using a paint program. The images and masks were analyzed together with a feature measurement algorithm that was written with Labview (National Instruments, Austin, Tex) image-processing tools. Statistical analysis of the feature measurements was likewise performed by using the tools available with Labview.

Pathologic Review of Confocal Images

Multiple confocal images obtained at various depths were reviewed by 13 engineering graduate students and two biomedical engineering faculty members from the University of Texas at Austin and the University of Texas M.D. Anderson Cancer Center. The review was performed to determine whether individuals without formal training in pathology could diagnose dysplasia with confocal images. Each reviewer was asked to classify each biopsy specimen as normal or abnormal on the basis of a training set of cervical confocal images obtained from a previous study (15). Between three and eight images per biopsy were grouped into image sets. The reviewer knew from which patient each image set came but was blinded to histologic findings and colposcopic impression. Reviewers were informed that one biopsy specimen from each patient was obtained from a colposcopically normal site and one was obtained from a colposcopically abnormal site but that the histopathologic diagnoses of the pair could identify both as normal, both as abnormal, or one as abnormal and one as normal. The sensitivity and specificity of each reviewer's diagnosis was calculated by using the histopathologic finding as the standard of reference. Similarly, the sensitivity and specificity of the colposcopic impression were calculated.

RESULTS

Figure 2 shows images of colposcopically normal and abnormal biopsy specimens obtained in one patient at various depths. The cell nuclei can be seen on all of the confocal images, and the cell outlines can be seen around most cells of the normal specimen. The nuclear density of the abnormal specimen is clearly increased compared with that of the normal specimen. The area of individual nuclei on the images of the abnormal specimen is also greater than that of the normal specimen. These differences, which are evident at the top of the specimens, are sugges-

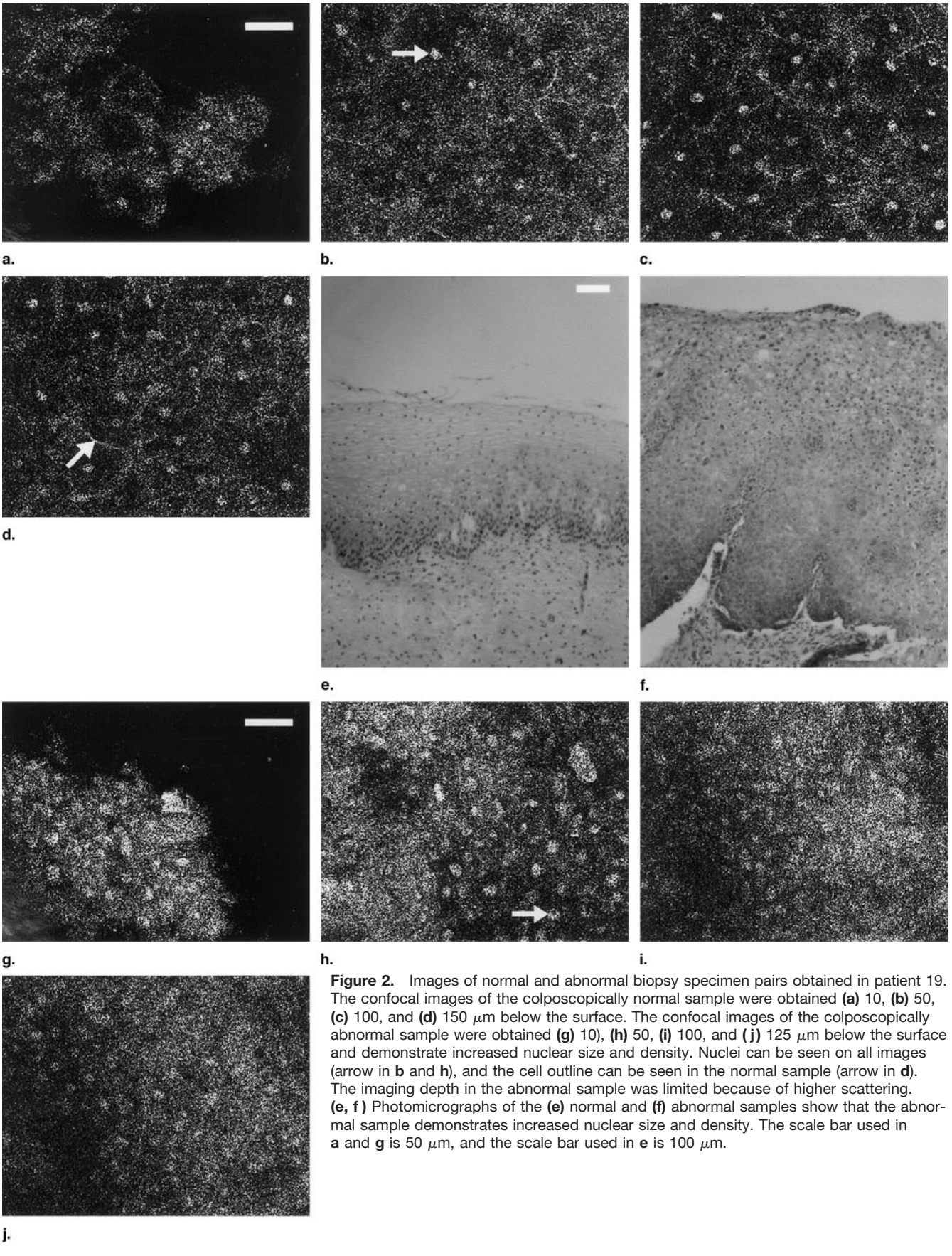

Figure 2. Images of normal and abnormal biopsy specimen pairs obtained in patient 19. The confocal images of the colposcopically normal sample were obtained **(a)** 10, **(b)** 50, **(c)** 100, and **(d)** 150 μm below the surface. The confocal images of the colposcopically abnormal sample were obtained **(g)** 10), **(h)** 50, **(i)** 100, and **(j)** 125 μm below the surface and demonstrate increased nuclear size and density. Nuclei can be seen on all images (arrow in **b** and **h**), and the cell outline can be seen in the normal sample (arrow in **d**). The imaging depth in the abnormal sample was limited because of higher scattering. **(e, f)** Photomicrographs of the **(e)** normal and **(f)** abnormal samples show that the abnormal sample demonstrates increased nuclear size and density. The scale bar used in **a** and **g** is 50 μm, and the scale bar used in **e** is 100 μm.

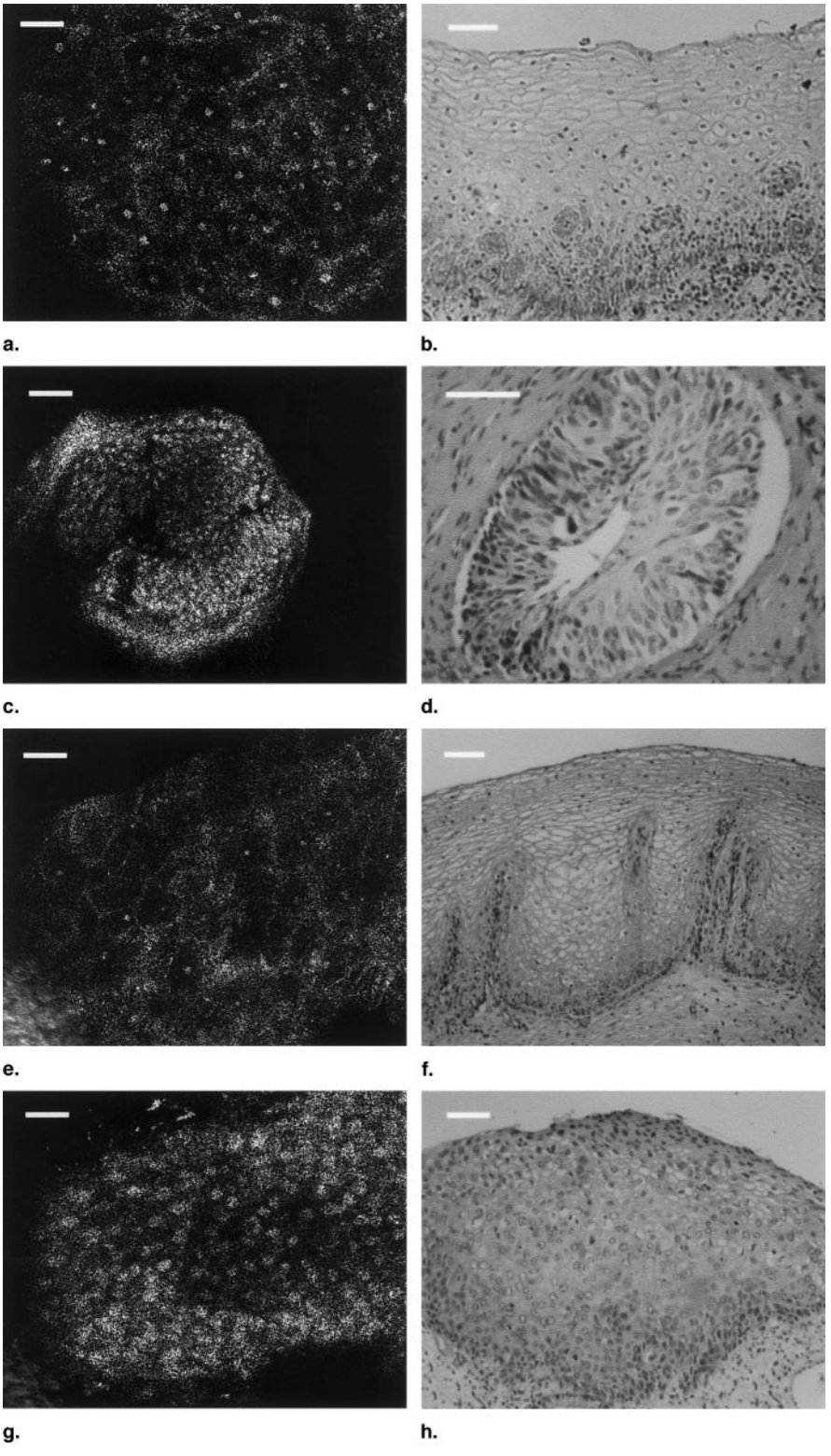

Figure 3. **(a, c, e, g)** Confocal images and **(b, d, f, h)** photomicrographs of normal **(a, b, e, f)** and abnormal **(c, d, g, h)** specimen pairs from patients 9 and 12 (**a–d** and **e–h**, respectively). Increased nuclear density can be seen on the confocal images of the abnormal samples (**c**, **g**). The confocal images were obtained 50 μm below the surface. At histologic examination, the specimens were classified as normal (**b**, **f**) and as having CIN II and/or III (**d, h**). The scale bar used for the confocal images is 50 μm, and the scale bar used for the histologic images is 100 μm.

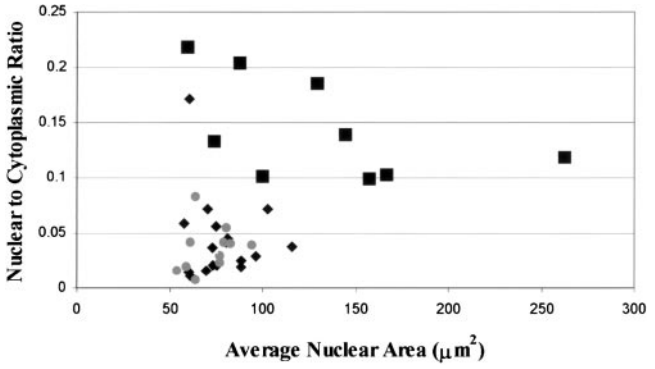

Figure 4. Graph shows comparison of the nuclear-cytoplasmic ratio to the average nuclear area for biopsy specimens classified as normal (◆), CIN I (●), or CIN II and/or III (■) on the basis of pathologic review. Measurements were calculated from images obtained 50 μm below the tissue surface. Normal and CIN I samples are localized to the area on the graph with lower nuclear-cytoplasmic ratio and smaller nuclear area. The differentiation between classes with the nuclear-cytoplasmic ratio is better than that with nuclear area.

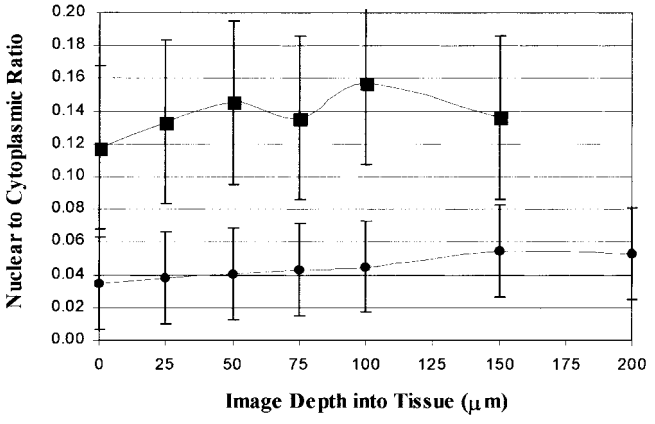

Figure 5. Graph shows the nuclear-cytoplasmic ratio as a function of depth for biopsy specimens classified as normal or CIN I (●) or CIN II and/or III (■) by means of pathologic review.

tive of the presence of cervical intraepithelial neoplasia (CIN) III in the abnormal specimen. Results of pathologic review of the abnormal specimen helped confirm this diagnosis. The maximum depth at which images could be obtained (penetration depth) also differed between these normal and abnormal specimens. This is likely due to differences in scattering of light both to and from the image plane. The image of the abnormal specimen (Fig 2d) obtained 125 μm below the surface is the deepest at which subcellular detail can been visualized in this biopsy specimen; however, subcellular detail was visualized on images of the normal biopsy specimen obtained up to a depth of 250 μm (not shown). This difference in scattering between normal and abnormal tissue could potentially provide another quantifiable measurement of contrast between normal and dysplastic tissue.

Figure 3 shows image pairs from two patients and the corresponding histologic images. In this case, all confocal images shown were obtained 50 μm below the surface. In each biopsy pair, the difference in nuclear density and area between the colposcopically normal and colposcopically abnormal specimens is evident. The change in nuclear density between the normal and abnormal confocal image pairs is highlighted because of the orientation of the confocal images, which are perpendicular to those of typical histologic sections. Architectural similarities are also evident between the confocal and histologic images, particularly in the images of dysplastic squamous epithelium that has involved a gland (Fig 3c, 3d). In this one confocal-histologic image pair, the image orientation is the same.

We reviewed the nuclear morphometric measurements extracted from the confocal images to determine whether any diagnostic contrast can be realized, and, if so, which features are most important. Figure 4 shows a scatterplot in which the average nuclear area from each biopsy is compared with the nuclear-cytoplasmic ratio from the same image. Each image was obtained 50 μm below the biopsy surface. A grouping of the normal specimens and those with CIN I is clearly localized in the lower left quadrant. A distinction between normal specimens and those with CIN I from those with CIN II and III can be observed with nuclear-cytoplasmic ratios less than and greater than 0.08, respectively. No clear division line can be drawn to segment these classes according to nuclear area. Both nuclear area and nuclear-cytoplasmic ratio appear to contribute to the distinction between sample types; however, the nuclear-cytoplasmic ratio clearly enables better differentiation between the two classes. The nuclear-cytoplasmic ratio also enabled better differentiation of the tissue classes than did nuclear density (not shown).

Figure 5 shows the average nuclear-cytoplasmic ratio for all biopsy specimens as a function of image depth. The error bar at each data point is a measure of two times the standard deviation of the nuclear-cytoplasmic ratio for images obtained at that depth. A clear division can be seen between specimens diagnosed as CIN II and/or III and those diagnosed as CIN I or normal. If the specimens with nuclear-cytoplasmic ratios greater than 0.08 are categorized as CIN II and/or III and those with ratios lower than 0.08 as CIN I or normal and these measurements are compared with the results of pathologic examination, the

sensitivity and specificity of this classification method is 100% and 91%, respectively.

Figure 6 shows the results of the diagnoses made by the untrained reviewers. The average sensitivity and specificity are 95% and 69%, respectively. Ten of the reviewers classified samples with a sensitivity of 100%; the remainder classified samples with a sensitivity of 89%. The specificity varied from 50% to 76% (standard deviation, ±8%). None of the reviewers had a sensitivity or specificity that approached that of quantitative analysis. The sensitivity and specificity of colposcopic appearance compared with histopathologic diagnosis were 91% and 62%, respectively. The colposcopic and histopathologic diagnoses of the biopsy specimens are shown in the Table. Specimens with a pathologic diagnosis of inflammation and metaplasia were classified as normal in the sensitivity and/or specificity calculations; specimens with a pathologic diagnosis of koilocytosis were classified as having CIN I.

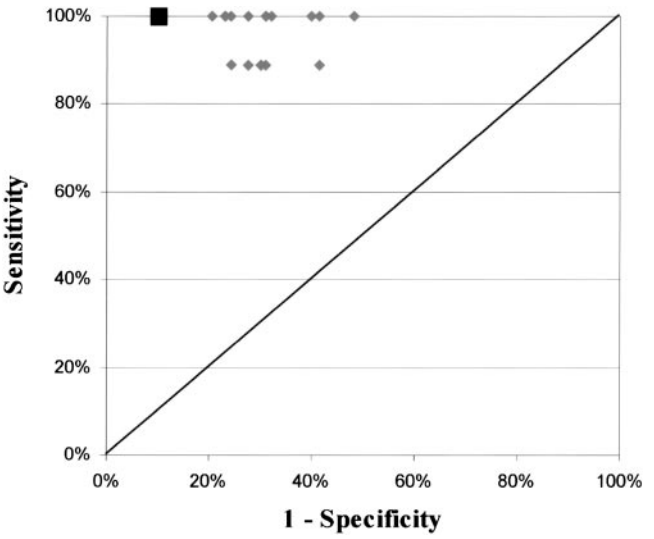

Figure 6. Graph shows the sensitivity and specificity of the diagnoses made by the untrained reviewers (◆) and with quantitative analysis of the nuclear-cytoplasmic ratio (■). The average sensitivity and specificity of the untrained reviewers (95% and 69%, respectively) are an improvement over that with colposcopy. The sensitivity and specificity is improved with quantitative analysis (100% and 91%, respectively).

DISCUSSION

Our results show that both quantitative analysis of confocal images and qualitative review by untrained observers can yield high sensitivity and specificity compared with histopathologic diagnosis. Analysis of nuclear feature measurements indicated that the nuclear-cytoplasmic ratio appears to be the most important feature for detecting dysplasia on confocal images in which the image plane is parallel to the tissue surface. The penetration depth at which images with clear intracellular features could be obtained was limited to the upper half of the epithelium in biopsy specimens with high-grade dysplasia; however, we were still able to diagnose these biopsy specimens accurately.

To our knowledge, the high sensitivity and specificity of the system measured quantitatively are extremely promising and exceed most values reported from systems designed for the in vivo detection of dysplasia. Furthermore, the qualitative analysis of the confocal images by the untrained reviewers provides an improvement over the macroscopic review of the tissue by using colposcopy. The sensitivity and specificity of colposcopy for this study are 91% and 62%, respectively, which are higher than those reported in a previous study (17). The 69% specificity of the untrained reviewers is also likely lower than might be measured with a more evenly distributed population of normal and abnormal biopsy specimens. Many more biopsy specimens were diagnosed by the pathologist as normal than abnormal (29 vs nine). This most likely resulted in a bias in the untrained reviewers toward increased false-negative findings.

These results indicate the potential of our fiberoptic confocal endoscope, which has a similar axial resolution (5–6 μm) and enables imaging in near real time. The primary difference between the fiberoptic confocal endoscope and the present system is the addition of the fiberoptic imaging bundle, which decreases signal throughput and introduces background noise from reflections of the fiber faces. These constraints are being overcome by using index matching oils to remove the specular reflection and increase throughput; we recently obtained in vivo images of the oral cavity by using the fiberoptic confocal microscope and achieved sufficient contrast to visualize subcellular detail (K. B. Sung, unpublished data, 2001).

The performance of the present system is comparable to that of in vivo video rate confocal imaging performed with a system used to image the oral mucosa (18) and human skin (10). The axial and lateral resolution of the present system (lateral resolution, 0.8 μm; axial resolution, 3–4 μm) compare well with those of the other system (lateral resolution, 0.5–1.0 μm; axial resolution, 3–5 μm). The cell features on the images shown herein are different than those of human skin (10), in which contrast originates from increased backscattering from melanin within the cytoplasm (8) and results in a relatively dark

Table
Colposcopic Appearance and Histopathologic Diagnosis for Each Biopsy Specimen

Patient No. and Biopsy Sample	Colposcopic Appearance	Histopathologic Diagnosis
Patient 1		
Sample A	Abnormal	Metaplasia
Sample B	Normal	Normal
Patient 2		
Sample A	Normal	Normal
Sample B	Abnormal	Normal
Patient 3		
Sample A	Abnormal	Koilocytosis
Sample B	Normal	Koilocytosis
Patient 4		
Sample A	Abnormal	Koilocytosis
Sample B	Normal	Normal
Patient 5		
Sample A	Normal	Normal
Sample B	Abnormal	CIN I
Patient 6		
Sample A	Normal	Normal
Sample B	Abnormal	Metaplasia
Patient 7		
Sample A	Normal	Normal
Sample B	Abnormal	CIN I
Patient 8		
Sample A	Abnormal	Koilocytosis
Sample B	Normal	Koilocytosis
Patient 9		
Sample A	Normal	Normal
Sample B	Abnormal	CIN II
Patient 10		
Sample A	Abnormal	CIN II
Sample B	Normal	CIN I
Patient 11		
Sample A	Normal	Normal
Sample B	Abnormal	Cancer
Patient 12		
Sample A	Abnormal	Inflammation
Sample B	Normal	Normal
Patient 13		
Sample A	Normal	Koilocytosis
Sample B	Abnormal	Koilocytosis
Patient 14		
Sample A	Abnormal	CIN II
Sample B	Normal	CIN I
Patient 15		
Sample A	Abnormal	Invasive carcinoma
Sample B	Normal	High-grade dysplasia
Patient 16		
Sample A	Normal	Normal
Sample B	Abnormal	CIN II
Patient 17		
Sample A	Abnormal	Metaplasia
Sample B	Normal	Metaplasia
Patient 18		
Sample A	Abnormal	CIN II/III
Sample B	Normal	Normal
Patient 19		
Sample A	Normal	Normal
Sample B	Abnormal	CIN II/III

(*continues*)

nucleus. On the current images, the contrast originates from increased backscattering from the nucleus owing to the interaction of acetic acid and the nucleus (14). Our images are similar to those obtained by Whitte et al (18) in the oral mucosa at superficial imaging depths but different deeper within the epithelium where nuclei visualized within the oral mucosa are dark, similar to that in human skin. The contrast provided with acetic acid has three primary advantages. After the application of acetic acid, the increased backscattering is uniform for virtually all nuclei in the field of view; nuclei can be visualized on images obtained at the bottom of the epithelium; and the edge between the nucleus and cytoplasm is distinct. These three characteristics enable improved quantitative measurements throughout the epithelium.

In the differentiation between high-grade dysplasia (CIN II and/or III) and low-grade dysplasia or normal tissue, the sensitivity and specificity of the system's quantitative feature measurements (100% and 91%, respectively) compare well with those of quantitative pathologic examination (N. Poulin, unpublished data, 1995). In quantitative pathology, measurements of cellular and nuclear morphometric and architectural features from histologic slides are used to make a diagnosis. By using a morphometric index calculated with multiple nuclear morphologic measurements of archived histologic slides, Poulin's group obtained a sensitivity of 90% and a specificity of 90%. The higher resolution and contrast from the stains allow many more types of morphometric measurements than those made from the confocal images. The obvious advantage of the confocal system is its ability to provide in vivo images.

The ability to image in vivo suggests the system's use in the diagnostic clinic. The high specificity of the instrument suggests its use for facilitating physicians' decisions about where to obtain colposcopic biopsy specimens. Many unnecessary biopsy specimens are obtained because of the relatively low specificity of colposcopy. The use of the instrument for guiding biopsy could result in greater convenience to the patient and lower costs in diagnostic procedures.

Another use of the instrument might be to aid in the study of progression and regression of precancerous tissue in chemoprophylaxis trials by tracking biomarkers. For example, there are ongoing chemoprevention trials in which retinoic acids are used to reverse precancerous lesions in the oral cavity and prevent second primary tumors in patients who have successfully completed treatment for head and neck cancers (19). Patients who have developed a head and neck cancer are very prone to a second primary cancer because the entire epithelial lining is at risk for neoplastic changes (field effect). To evaluate the effectiveness of these agents, multiple biopsy specimens must be obtained over time to evaluate the tissue at risk. The biopsy process itself, however, affects the field: Small foci of precancerous cells may be removed, and the resulting repair process disrupts the field. Further, many patients hesitate to enroll in such trials because of the multiple biopsies. In vivo optical imaging modalities such as confocal microscopy, which can enable the visualization of cells and nuclei throughout the epithelium and provide information about nuclear size and texture features, may enable the field at risk to be monitored without the need for biopsy, providing a powerful new tool to aid in chemoprevention studies.

We are continuing our analysis of images obtained deeper into the tissue to differentiate between low-grade dysplasia and normal tissue; however, the variation in penetration depth limits the number of biopsy specimens that can be imaged near the basement membrane. A larger study would provide adequate sample numbers to study these lesions. We are also studying the effect that changes in the scattering coefficient might have on the diagnostic sensitivity of the system. Future plans include in vivo imaging of the cervix with the fiberoptic confocal microscope. The present results indicate the clinical potential of in vivo confocal imaging.

REFERENCES

1. Parkin DM, Pisani P, Ferlay J. Estimates of the worldwide incidence of eighteen major cancers in 1985. Int J Cancer 1993; 54:594–606.
2. Kurman RJ, ed. Blaustein's pathology of the female genital tract. 4th ed. New York, NY: Springer-Verlag, 1994.
3. Jester V, Andrews PM, Petroll WM, Lemp MA, Cavanaugh HD. In vivo, real-time confocal imaging. J Electron Microsc Tech 1997; 18:50–60.
4. Jester V, Petroll WM, Garana RM, Lemp MA, Cavanaugh HD. Comparison of in vivo and ex vivo cellular structure in rabbit eyes detected by tandem scanning microscopy. J Microsc 1992; 165:169–181.
5. Masters B, Thaer AA. Real-time scanning slit confocal microscopy of the in vivo human cornea. Appl Opt 1994; 33:695–701.
6. Bertrand C, Corcuff P. In vivo spatio-temporal visualization of the human skin by real-time confocal microscopy. Scanning 1994; 16:150–154.
7. Corcuff P, Gonnord G, Pierard GE, Leveque JL. In vivo microscopy of human skin: a new design for cosmetology and dermatology. Scanning 1996; 18:351–355.
8. Rajadhyaksha M, Grossman M, Esterowitz D, Webb RH, Anderson RR. In vivo confocal scanning laser microscopy of human skin: melanin provides strong contrast. J Invest Dermatol 1995; 104:946–952.
9. Masters BR, Aziz UI, Gmitro AF, Kerr JH, O'Grady TC, Goldman L. Rapid observation of unfixed, unstained human skin biopsy specimens with confocal microscopy and visualization. J Biomed Opt 1998; 2:437–445.
10. Rajadhyaksha M, Gonzalez S, Zavislan J, Anderson RR, Webb RH. In vivo confocal scanning laser microscopy of human skin. II. Advances in instrumentation and comparison with histology. J Invest Dermatol 1999; 104:946–952.
11. Collier TG, Smithpeter CL, Descour M, Richards-Kortum, R. Fiber-optic confocal microscope for biological imaging. Presented at the 1998 Conference on Lasers and Electro-Optics, (CLEO), San Francisco, Calif, May 3–8, 1998.
12. Smithpeter CL, Dunn AK, Welch AI, Richards-Kortum R. Penetration depth limits of in vivo confocal reflectance imaging. Appl Opt 1998; 37:2749–2754.
13. Smithpeter CL, Dunn AK, Drezek R, Collier T, Richards-Kortum R. Near real time confocal microscopy of cultured amelanotic cells: sources of signal, contrast agents and limits of contrast. J Biomed Opt 1998; 3:429–436.
14. Drezek R, Collier T, Brookner C, et al. Laser scanning confocal microscopy of cervical tissue, before and after application of acetic acid. Am J Obstet Gynecol 2000; 182:1135–1139.
15. Collier T, Shen P, de Pradier B, Sung K, Richards-Kortum R. Near real time confocal microscopy of amelanotic tissue: dynamics of aceto-whitening enable nuclear segmentation. Opt Express 2000; 6:40–48. Available at: *http://www.opticsexpress.org*
16. Burke L, Antonioli D, Durcatman B. Colposcopy text and atlas. Appleton & Lange, 1991.
17. Mitchell MF, Schottenfeld D, Tortolero-Luna G, Cantor SB, Richards-Kortum R. Colposcopy for the diagnosis of squamous intraepithelial lesions: a meta-analysis. Obstet Gynecol 1998; 91:626–631.
18. Whitte WM, Ragadhyaksha M, Gonzalez S, Fabian RL, Anderson RR. Noninvasive imaging of human oral mucosa in vivo by confocal reflectance microscopy. Laryngoscope 1999; 109:1709–1717.
19. Mao L, El-Naggar AK, Papadimitrakopoulou V, et al. Phenotype and genotype of advanced premalignant head and neck lesions after chemopreventive therapy. J Natl Cancer Inst 1998; 90:1545–1551.